Applied Catalysis B: Environmental 343 (2024) 123573

Contents lists available at ScienceDirect

Applied Catalysis B: Environmental

journal homepage: www.elsevier.com/locate/apcatb

# Bacterial inactivation in sunlit surface waters is dominated by reactive species that emanate from the synergy between light, iron, and natural organic matter

Da Wang [a], Liwen Cai [a], Shuang Song [a], Stefanos Giannakis [b,*], Jun Ma [c], Davide Vione [d], Cesar Pulgarin [e,f,g,**]

[a] Key Laboratory of Microbial Technology for Industrial Pollution Control of Zhejiang Province, College of Environment, Zhejiang University of Technology, Hangzhou 310032, China
[b] Universidad Politécnica de Madrid (UPM), E.T.S. de Ingenieros de Caminos, Canales y Puertos, Departamento de Ingeniería Civil: Hidráulica, Energía y Medio Ambiente, Unidad docente Ingeniería Sanitaria, c/ Profesor Aranguren, s/n, ES-28040, Madrid, Spain
[c] State Key Laboratory of Urban Water Resource and Environment, School of Environment, Harbin Institute of Technology, Harbin 150090, China
[d] Dipartimento di Chimica, Università di Torino, Via P. Giuria 5, 10125, Torino, Italy
[e] School of Basic Sciences (SB), Institute of Chemical Science and Engineering (ISIC), Group of Advanced Oxidation Processes (GPAO), École Polytechnique Fédérale de Lausanne (EPFL), Station 6, CH-1015 Lausanne, Switzerland
[f] Grupo de Investigación en Remediación Ambiental y Biocatálisis (GIRAB), Instituto de Química, Facultad de Ciencias Exactas y Naturales, Universidad de Antioquia UdeA, Calle 70 No. 52–21, Medellín, Colombia
[g] Colombian Academy of Exact, Physical and Natural Sciences, Carrera 28 A No. 39A-63, Bogotá, Colombia

ARTICLE INFO

*Keywords:*
Solar disinfection (SODIS)
Iron
Natural organic matter
Synergistic effect
Reactive oxygen species

ABSTRACT

In this study, the synergistic and antagonistic effects of Fe species and coexisting natural organic matter (NOM) on the efficacy of solar light disinfection of water are investigated. Different initial iron species ($Fe^{2+}$/$Fe^{3+}$) and naturalorganic matter types (Suwannee River-SRNOM, Nordic Reservoir NOM-NDNOM, SR Humic Acid-SRHA, and SR Fulvic Acid-SRFA) were selected. The bactericidal actions of Fe and NOM, alone or in conjunction, were evaluated at various initial iron dosing concentrations, NOM concentrations, irradiation intensities, and pH values. We show that when an appropriate iron (1 ppm $Fe^{2+}$ or 0.25 ppm $Fe^{3+}$) and NOM concentration (2 ppm SRNOM or 5 ppm NDNOM) coexisted, synergistic inactivation was observed in the pH range 5.0–8.0. A plausible explanation is that the presence of Fe+NOM significantly promoted the generation of hydroxyl radicals ($^{\bullet}OH$) and singlet oxygen ($^1O_2$), which led to enhanced disinfection rates. These results elucidate the previously understudied effects of ubiquitous elements in natural waters and their impact on solar-mediated bacterial inactivation.

## 1. Introduction

The bactericidal effect of solar light has been known for centuries; however, over the last 40 years, it has been systematically exploited as a point-of-use water disinfection process [1]. Solar water disinfection (SODIS) has been approved by the World Health Organization (WHO) as a safe, stable, cheap, and efficient method for drinking water [2]. The basic SODIS technique usually involves placing water in a transparent container and exposing it to direct sunlight for at least 6 h before it is ready to drink [1]. The bactericidal action of SODIS is based on the synergistic effect of UVA radiation and temperature increase [3]. Natural organic matter (NOM), a ubiquitous water component, has received increasing attention because of its multiple roles in SODIS. For instance, NOM can act as a sensitizer in aquatic systems by generating a series of photoinduced reactive intermediates (PPRIs) after light absorption [4]. PPRIs include reactive oxygen species (ROS) such as singlet oxygen ($^1O_2$), superoxide radical anions ($O_2^{\bullet-}$), hydrogen peroxide ($H_2O_2$), and hydroxyl radicals ($^{\bullet}OH$), as well as the triplet state of NOM ($^3$NOM*).

* Corresponding author.
** Corresponding author at: School of Basic Sciences (SB), Institute of Chemical Science and Engineering (ISIC), Group of Advanced Oxidation Processes (GPAO), École Polytechnique Fédérale de Lausanne (EPFL), Station 6, CH-1015 Lausanne, Switzerland.
*E-mail addresses:* Stefanos.Giannakis@upm.es (S. Giannakis), Cesar.Pulgarin@epfl.ch (C. Pulgarin).

https://doi.org/10.1016/j.apcatb.2023.123573
Received 17 January 2023; Received in revised form 11 September 2023; Accepted 26 November 2023
Available online 29 November 2023

These PPRIs inactivate pathogens and degrade organic contaminants [5]. However, NOM has also been shown to absorb sunlight UV radiation, inhibit organic contaminant oxidation, and act as a scavenger of some PPRIs such as $^{\bullet}OH$ [6]. Therefore, when studying other factors in SODIS or solar-induced systems, it is important to consider the effects of the NOM type and concentration.

The photo-Fenton process is a hot research topic that has been extensively investigated in recent years [7]. Normally, iron acts as a catalyst and reacts with $H_2O_2$ to produce $^{\bullet}OH$, which has bactericidal effect [8–10]. However, low iron solubility at near-neutral pH inhibits the disinfection efficiency of the photo-Fenton reaction [11]. Previous studies have also shown that NOM significantly affects disinfection via induction of the photo-Fenton process [12–14]. In such circumstances NOM forms complexes with iron [15], thereby inhibiting the transformation of homogeneous iron ions into heterogeneous iron compounds. Therefore, the presence of dissolved iron contributes to the maintenance of an effective Fenton cycle [16,17]. Furthermore, NOM-$Fe^{3+}$ complexes undergo ligand-to-metal charge transfer (LMCT) under sunlight, which photo-reduces $Fe^{3+}$ to $Fe^{2+}$ and activates $H_2O_2$ to produce free radicals [18]. This phenomenon can enhance the bactericidal action of SODIS [19]. At the same time, NOM absorbs sunlight and scavenges $^{\bullet}OH$ [6], with the potential to inhibit the photo-Fenton processes.

Previous studies have mainly focused on the activation of $H_2O_2$ by promoting $Fe^{2+}/Fe^{3+}$ cycling during LMCT. However, other possible effects of Fe on bacteria remain largely unexplored. Moreover, the photo-Fenton process requires the addition of Fenton reagents (Fe/$H_2O_2$), which could be an issue for resource-poor communities [20]. Although Fe can be obtained from locally available materials, there may be problems with the supply of $H_2O_2$. In addition, owing to the poor solubility of ferric species, this process is expected to achieve high efficiency only at acidic pH values [21]. Therefore, a tradeoff between efficiency and feasibility remains.

NOM in natural water can stabilize iron ions; however, excessive NOM competes with bacteria to scavenge generated PPRIs [22,23]. Considering the various possible effects of NOM on the SODIS process and the significant effect of pH on iron speciation, it can be predicted that the bacterial disinfection performance of SODIS is significantly affected by the simultaneous presence of iron and NOM. To the best of our knowledge, despite previous efforts, these remain unanswered questions that require systematic investigation.

In this study, we focused on elucidating the possible synergistic or antagonistic effects of NOM and Fe species on the bactericidal efficacy of SODIS. First, the effects of NOM and Fe on bacterial inactivation were investigated. Four different types of NOM were selected: Suwannee River NOM (SRNOM), Suwannee River Humic Acid (SRHA), Suwannee River Fulvic Acid (SRFA), and Nordic Reservoir NOM (NDNOM). These models were used to investigate bacterial inactivation at various NOM concentrations, irradiation intensities, and pH values. The effects of the initial iron species ($Fe^{2+}$ and $Fe^{3+}$) and their dosage on the SODIS performance at different pH values were investigated to determine the optimal iron concentration. The combined bactericidal effect of Fe and NOM was systematically investigated as a function of pH, and important information was obtained by analyzing the NOM-specific spectral parameters. The synergistic and antagonistic effects of Fe and NOM were evaluated by comparing their combined presence with that of the separate components, with a special focus on PPRI generation. Finally, an integrated mechanism for bacterial inactivation was proposed.

## 2. Materials and methods

The chemical reagents used are described in Supplementary Text S1. Bacterial inactivation experiments took place in 50 mL UVB- and UVA-transparent Pyrex glass reactors that were placed on a magnetic stirrer (350 rpm). An Atlas XLS Suntest solar simulator system equipped with an air-cooled xenon lamp with a controllable output solar intensity ($\lambda >$ 290 nm) was employed for the experiments, similar to [24]. Throughout the study, the reaction temperature was below 30 °C.

In a typical experiment, stationary-phase *E. coli* was added to each reactor from overnight cultures, diluted to the initial experimental concentration ($\sim 10^6$ CFU $mL^{-1}$), and stirred. Text S2 summarizes the preparation method, but for a detailed protocol of *E. coli* preparation, interested readers can refer to [25].

The initial pH of the solution was adjusted by the addition of HCl or NaOH (1 mM). After stirring for 30 min, predetermined amounts of iron and/or NOM were introduced into the reactor and irradiation was started immediately. At defined time intervals, samples (1 mL) were withdrawn to determine the concentration of the cultivable bacteria.

Analytical methods, including measurements of the total organic carbon (TOC) of NOM solutions and concentrations of furfuryl alcohol (FFA) and 2,4,6-trimethylphenol (TMP) (see [25]), are described in Text S3. The contribution of each PPRI generated under irradiation, including $^{\bullet}OH$, $^3NOM^*$ , and $^1O_2$, was calculated according to the methods described in Text S4 and those previously reported by Kohantorabi et al. [25], Ma et al. [26], and Vione et al. [27].

## 3. Results and discussion

To identify the role and contribution of each iron species ($Fe^{2+}$ or $Fe^{3+}$) and the type and origin of NOM (SRNOM, NDNOM, SRHA, and SRFA) to bacterial inactivation, the effects of the following components were investigated: i) NOM upon irradiation (Section 3.1), ii) iron species upon irradiation (Section 3.2), and iii) iron + NOM upon irradiation (Section 3.3). Sections 3.4–3.5 present the results of spectral characterization and PPRI generation resulting from the association of Fe with NOM, and Section 3.6 proposes an integrated mechanism of bacterial inactivation.

### 3.1. The influence of NOM on SODIS

As a first step in this investigation, we studied the effects of NOM alone and irradiance on SODIS in the absence of iron species. Various concentrations of SRNOM (0–5 ppm) and NDNOM (0–10 ppm) were used under 750 W $m^{-2}$ simulated sunlight irradiation. The results are shown in Fig. 1a and b, respectively.

The bacterial inactivation kinetics increased with an increasing SRNOM concentration in the TOC range of 0–1 ppm and reached a plateau at 2 ppm, resulting in a 4-log *E. coli* inactivation after 3 h of irradiation. In the absence of NOM (SODIS only), inactivation was close to 1-log. A similar phenomenon was observed in the presence of NDNOM; however, the plateau concentration was 5–7.5 ppm. Under

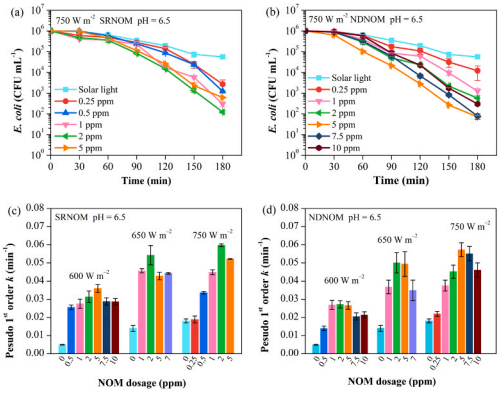


**Fig. 1.** Effects of (a) SRNOM and (b) NDNOM dosage on bacteria inactivation, and effects of light intensity on bacteria inactivation with various concentrations of (c) SRNOM, and (d) NDNOM (For (a) and (b): pH = 6.5, light intensity = 750 W $m^{-2}$, $[E.\ coli]_0 = 10^6$ CFU $cm^{-3}$; for (c) and (d): pH = 6.5, $[E.\ coli]_0 = 10^6$ CFU $cm^{-3}$, $[NOM]_0$ = 0.25–10 ppm).

these conditions, we obtained 4-log *E. coli* inactivation as well. Therefore, at SRNOM and NDNOM concentrations of 2 ppm (SRNOM) and 5 ppm (NDNOM), bacterial inactivation was enhanced rather than inhibited.

The increase in bacterial inactivation with increasing NOM concentrations has been attributed to energy transfer and transient species generation [28]. NOM has been widely studied as a photosensitizer; sunlight absorption by NOM generates excited states (including triplet state $^3$NOM*), which also causes charge separation ($NOM^{\bullet+/\bullet-}$) [29]. In the triplet state, $^3$NOM* can undergo energy transfer to molecular oxygen and promote $^1O_2$ generation, whereas $O_2^{\bullet-}$ can be produced by electron transfer from $NOM^{\bullet-/\bullet+}$ to molecular oxygen, which eventually yields $H_2O_2$. All these species participate in diverse intracellular processes, resulting in enhanced bacterial inactivation [30].

Interestingly, bacterial inactivation performance declined slightly at high concentrations of SRNOM (5 ppm) and NDNOM (10 ppm), as shown in Figs. 1a and 1b, likely due to the potential competition for light absorption between NOM and bacteria, and possibly to PPRI scavenging by NOM [31]. Therefore, NOM in the solution acts as an antagonist or agonist of SODIS in a concentration-dependent manner.

To identify the role of light intensity, three levels were tested: 600 W m$^{-2}$, 650 W m$^{-2}$, and 750 W m$^{-2}$, in the presence of SRNOM or NDNOM. As shown in Figs. 1c and 1d, high irradiation intensity is more effective for *E. coli* inactivation than low light intensity [32–34]. Under dark conditions, the concentration of *E. coli* remained stable in the presence of NOM for 240 min (data not shown), suggesting that NOM had no inhibitory effect on *E. coli* when not irradiated [14]. In particular, the synergistic germicidal effect of solar UV radiation and heat is known to play an important role in SODIS [35]. Heat-induced bacterial inactivation is negligible at temperatures below 30 °C, whereas temperatures above this threshold enhance inactivation rates [36]. In our study, the reaction temperature was below 30 °C throughout the study; thus, heat was not a major factor for bacterial inactivation. UVB radiation damages a diverse range of cellular components, resulting in severe dysfunction of microorganisms and leading to their inactivation when radiation is directly absorbed by DNA [14]. Furthermore, evidence suggests that UVA radiation (320–400 nm) causes distinct types of damage and acts directly on DNA through one-electron oxidation reactions and $^1O_2$ processes [37–40]. These phenomena explain why bacterial inactivation increases with increasing irradiance in the absence of NOM.

The effect of irradiance on bacterial inactivation is more apparent in the presence of NOM. Light intensities of 600 W m$^{-2}$, 650 W m$^{-2}$, and 750 W m$^{-2}$ were chosen to study the role of NOM concentration in bacterial inactivation. As shown in Figs. 1c and 1d, increasing light intensity gradually enhanced bacterial inactivation in the presence of various concentrations of SRNOM and NDNOM, respectively. Trend details were not the same for the two NOM types, which might suggest somewhat different responsiveness to changes in light intensity.

To investigate the effect of the initial pH on bacterial inactivation in the presence of NOM, the apparent inactivation rate constants ($k_{app}$) were measured in the absence or presence of SRNOM and NDNOM in the pH range of 5.0–8.0 (Fig. 2a). The pH of the aqueous solution is an important factor in bacterial inactivation in SODIS. Blank experiments (in the dark) showed that the survival rate constant of *E. coli* remained stable in the pH range 5.0–8.0 (Fig. S1). In the absence of NOM, $k_{app}$ gradually decreases with increasing pH. On the one hand, higher concentrations of hydrogen ions can improve disinfection by promoting intracellular production of PPRIs [41]. Furthermore, an acidic solution presents significant additional stress to bacteria (especially under starved conditions, as per our tests), resulting in faster depletion of adenosine triphosphate (ATP), which requires cells to consume stored energy reserves to maintain pH homeostasis. In addition, acidic pH may reduce the metabolic rate of energy-consuming proteins in bacteria, which are normally capable of scavenging PPRIs and repairing damaged cell components [42]. As a result, the survivability of bacteria under harsh conditions (oxidative stress and UV radiation) is considerably impaired at an acidic pH.

Compared with SODIS in the absence of NOM, the addition of NOM maintained pH-dependent disinfection trends but clearly led to higher $k_{app}$ values. Similar effects were observed with 2 ppm SRNOM and 5 ppm NDNOM, which were identified as the NOM concentrations that produced the fastest disinfection in previous experiments at the same (750 W m$^{-2}$) light intensity (see Fig. 1c and d).

The disinfection ability of irradiated SRNOM was also compared with that of its separated humic (SRHA) and fulvic (SRFA) components. Among possible differences between SRNOM, SRHA, and SRFA, it has been reported that the contents in carboxylic groups of the three substances follow the order SRFA (12.23 meq $g_C^{-1}$) > SRNOM (9.85 meq $g_C^{-1}$) > SRHA (9.59 meq $g_C^{-1}$). Moreover, the contents of phenolic compounds are in reverse order: SRHA (4.24 meq $g_C^{-1}$) > SRNOM (3.94 meq $g_C^{-1}$) > SRFA (3.11 meq $g_C^{-1}$) [43].

As shown in Fig. 2b, SRHA and SRFA at different concentrations enhanced the inactivation of bacteria (by approximately 1 log or more) compared with the baseline solar damage. On the one hand, SRHA induced higher *E. coli* inactivation than SRFA; even in SRFA + SRHA mixtures, inactivation became faster when the SRHA fraction increased. At the same time, however, inactivation in the presence of both SRHA and SRFA was lower than inactivation in the presence of SRNOM (see comparable conditions in Figs. 2a and 2b). Our findings reveal two implications:

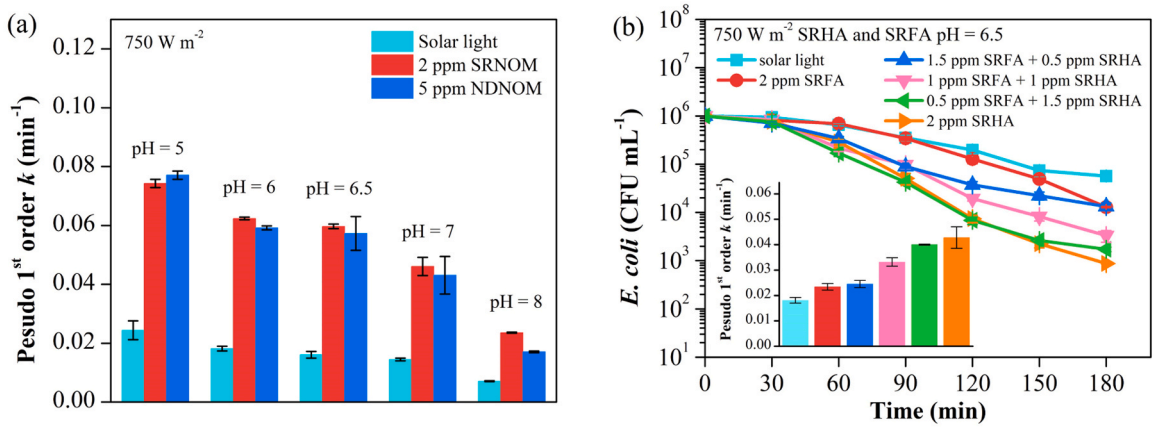


**Fig. 2.** Effects of (a) initial pH on bacterial inactivation in the presence of SRNOM and NDNOM, and (b) different ratios of SRHA and SRFA on the inactivation of bacteria (light intensity = 750 W m$^{-2}$, $[E. coli]_0 = 10^6$ CFU cm$^{-3}$).

(i) NOM components other than HA and FA likely played additional roles in bacterial photoinactivation. To gain further insight into this issue, the spectral properties of organic matter and their changes with irradiation were investigated (see Section 3.4).

(ii) The differences between SRHA and SRFA might confirm that phenolic moieties (more concentrated in SRHA than in SRFA) contribute to bacterial inactivation because of their strong electron-donor properties [44,45]. Most likely, electron transfer towards bacteria destabilizes the outer membrane, leading to inactivation.

### 3.2. The influence of iron species on SODIS

#### 3.2.1. Effect of Fe dosage and light intensity on SODIS

Fig. 3a shows the inactivation of *E. coli* under 750 W $m^{-2}$ light intensity with various concentrations of $Fe^{2+}$. The addition of $Fe^{2+}$ enhanced bacterial inactivation, and its effect was approximately 2-logU. Moreover, the optimum inactivation was achieved with 1 ppm $Fe^{2+}$, above which the effect of $Fe^{2+}$ decreased. $Fe^{2+}$ in an oxic environment is transformed into $Fe^{3+}$; hence, the effects of $Fe^{3+}$ on *E. coli* were investigated. The results are shown in Fig. 3b, where the effect of $Fe^{3+}$ was less marked than that of $Fe^{2+}$, and inactivation in the presence of $Fe^{3+}$ decreased considerably above 0.25 ppm.

Theoretically, iron species have complex effects on the photoinactivation of bacteria. At neutral pH, iron can be readily adsorbed on the surface of negatively charged *E. coli* cells or bonded with lipopolysaccharide molecules on the outer surface of bacterial membranes [13,46,47]. The redox reactions of iron in the solution or on the cell surface can cause •OH generation, and further production of PPRIs may be derived from photoinduced ligand-to-metal chain reactions [13,48–50].

Furthermore, $Fe^{2+}$ and $Fe^{3+}$ can be transported into metabolically active *E. coli* via various mechanisms. $Fe^{2+}$ assimilation is controlled by the *feo* system, or this ion can pass through the outer membrane porins into the bacterial cell because of its relatively low charge density and the difference in osmotic pressure between the cell and matrix [46,51,52]. $Fe^{3+}$ can bind to siderophores on the outer membrane of bacteria to form a complex that is then delivered into the cell through specific outer membrane receptors, with the help of another complex called TonB-ExbB-ExbD [46]. Once inside the cell, Fe acts as a catalyst for oxidative events. Fe can induce oxidative stress, cause DNA damage, and produce PPRIs through intracellular, photocatalytic, and internal Fenton reactions with photogenerated $H_2O_2$. These processes can cause multi-level cell damage [13,50].

Interestingly, iron concentrations above a certain level did not further enhance bacterial inactivation and were even detrimental to it (see Fig. 3). This finding can be tentatively explained by the fact that $Fe^{3+}$ tends to form insoluble precipitates at slightly acidic and near-neutral pH values, which can block light transmission and, therefore, decrease the SODIS performance.

Fig. 3c and d compare the effect of increasing light intensity (from 600 to 750 W $m^{-2}$) on the inactivation of bacteria. A higher intensity generally led to faster inactivation, but the observed trends with iron concentration were different in the two cases ($Fe^{2+}$ and $Fe^{3+}$, respectively). More photons are transmitted into the reaction system by increasing light intensity, which can accelerate the iron-assisted bacterial inactivation process. For example, UVA mediates the degradation of ferritin and other ferritin-like substances by disrupting their ligands, resulting in the immediate release of iron into the cell [53]. Increased

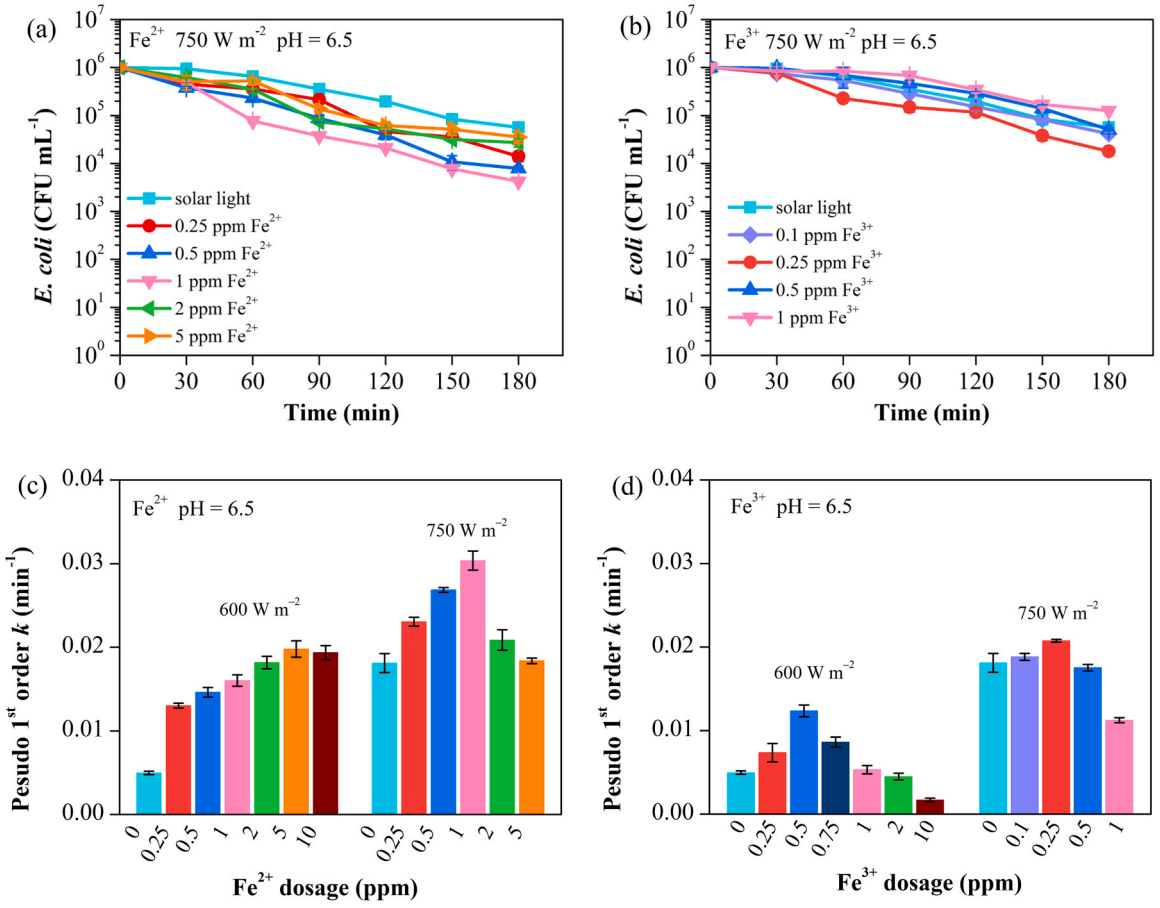


**Fig. 3.** Effects of (a) $Fe^{2+}$ and (b) $Fe^{3+}$ dosage on bacterial inactivation, and effects of light intensity under various concentrations of (c) $Fe^{2+}$ and (d) $Fe^{3+}$ (For (a) and (b): pH = 6.5, light intensity = 750 W $m^{-2}$, $[E.\ coli]_0 = 10^6$ CFU $cm^{-3}$, for (c) and (d): pH = 6.5, $[E.\ coli]_0 = 10^6$ CFU $cm^{-3}$, $[Fe]_0$ = 0.25–10 ppm).

light intensity also accelerates the photoreduction of $Fe^{3+}$ complexes and promotes the $Fe^{3+}/Fe^{2+}$ cycle, which enhances the photo-Fenton reaction in the cells. In addition, it enhances the photooxidation reactions (including Type I and Type II reactions) induced by UVA radiation. Type I reactions damage DNA through electron transfer, whereas Type II reactions generate singlet oxygen through energy transfer. Singlet oxygen has a longer half-life than hydroxyl radicals, and it reacts with many cellular macromolecules, including DNA, which results in DNA damage and ultimately leads to the inactivation of bacteria [54]. Finally, the results shown in Fig. 3 suggest that $Fe^{2+}$ showed more effective bacterial inactivation than $Fe^{3+}$ under all conditions, which could be attributed to the lower water solubility of the $Fe^{3+}$ species. Hence, in addition to the concentration, the speciation of iron is a key factor in disinfection and was further assessed.

### 3.2.2. Speciation of Fe during SODIS

To further explore the role of Fe species in the inactivation of bacteria, we tested different initial concentrations of $Fe^{2+}$ and $Fe^{3+}$ and monitored their temporal trends (Fig. 4). The experiments were performed in the presence or absence of bacteria to understand their contribution to Fe speciation and test the validity of our previous suggestions. The total concentration of iron species in the bacteria-containing suspension was measured directly without filtration (therefore, *E. coli* in such a case was not filtered out), while the concentrations of dissolved iron species were measured by first filtering out the bacteria, together with possibly occurring Fe precipitates.

***$Fe^{2+}$ addition***: Fig. 4a and b shows that the concentrations of $Fe^{2+}$ can be stabilized at a high level in the systems without generating much $Fe^{3+}$, no matter if the dosage of $Fe^{2+}$ is 0.5 ppm or 2 ppm. Moreover, the overall time trend of the iron species did not change significantly irrespective of the initial concentration of $Fe^{2+}$. It can be assumed that the change in $Fe^{2+}$ concentration in the reaction system is related to the bacterial inactivation process. For instance, the initial decrease in $Fe^{2+}$ concentration (first 30 min of the experiment) in the presence of *E. coli* was presumably due to the partial diffusion of $Fe^{2+}$ into the bacterial cells, which then tended to decrease.

Simultaneously, the parallel increase in $Fe^{3+}$ may be due to $O_2$-mediated oxidation and electron transfer from $Fe^{2+}$ to bacteria during SODIS. Subsequently, the concentration of dissolved $Fe^{3+}$ decreased to a low level (Fig. 4a and b).

We suggest that dissolved $Fe^{2+}$ first diffuses into the bacterial cells and causes internal oxidative processes under irradiation. These processes would oxidize $Fe^{2+}$ to $Fe^{3+}$, which then remains inside the bacterial cells or binds to bacterial membrane components. The generated $Fe^{3+}$ can quickly return $Fe^{2+}$ through the Fe-S cluster process, LMCT process, or other potential pathways under light, which keeps bacterial inactivation operational [55].

***$Fe^{3+}$ addition***: In the case of $Fe^{3+}$ addition (Fig. 4c and d), relatively high values of $Fe^{2+}$ were quickly detected in the system. $Fe^{3+}$ can be adsorbed onto the surface of bacteria or readily passed into the cell membrane with the aid of siderophore proteins, to form stable photoactive complexes. These complexes are known to participate in *E. coli* deactivation under irradiation and may reduce $Fe^{3+}$ to $Fe^{2+}$ [18]. The reduction process can occur on the bacterial surface or inside the cell and involves flavins, superoxide, or electrons produced during irradiation [18]. Interestingly, considerably lower $Fe^{2+}/Fe^{3+}$ ratios were observed when the initial $Fe^{3+}$ concentration was 2 ppm (Fig. 4d) compared to 0.5 ppm (Fig. 4c). This difference may be due to a shortage

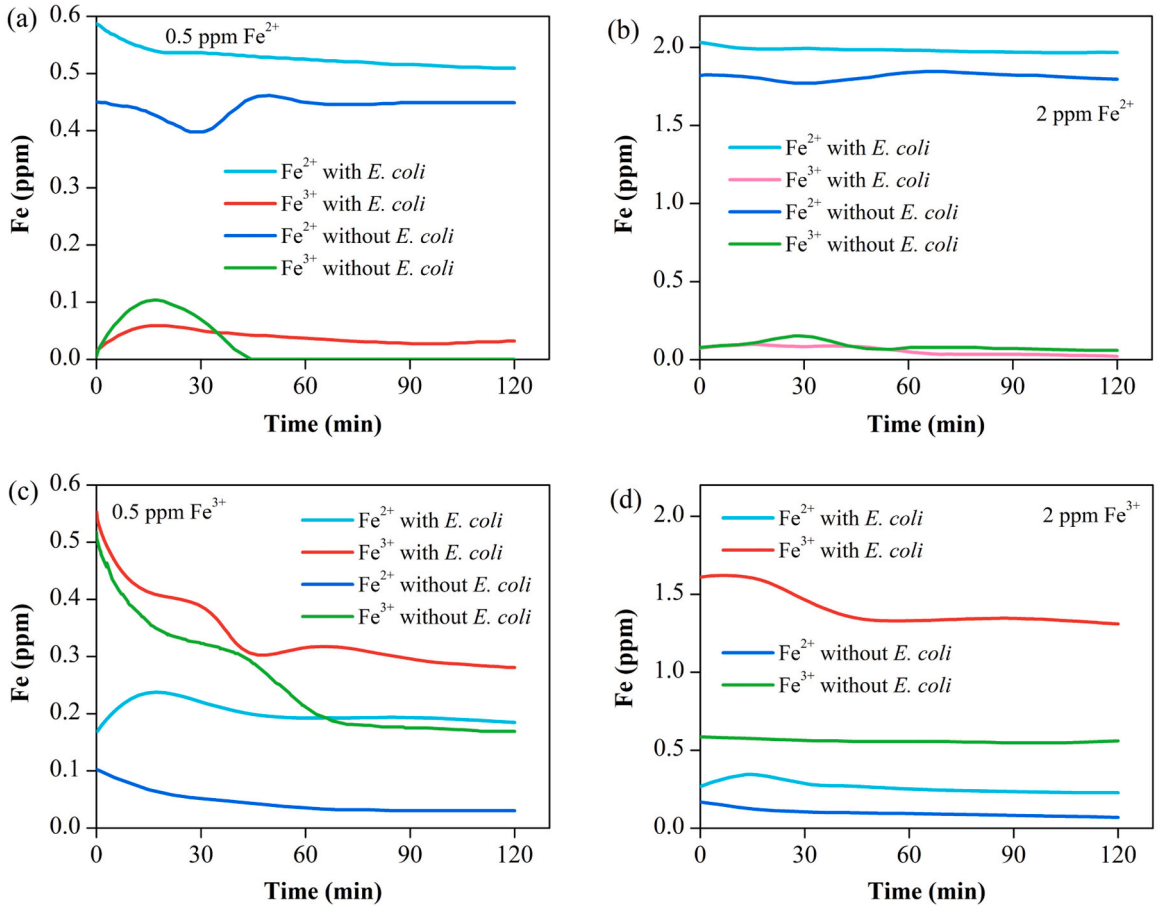


**Fig. 4.** Variation of the dissolved concentration of iron as a function of time upon irradiation with (a) 0.5 ppm $Fe^{2+}$, (b) 2 ppm $Fe^{2+}$, (c) 0.5 ppm $Fe^{3+}$ and (d) 2 ppm $Fe^{3+}$ (pH = 6.5, light intensity = 750 W $m^{-2}$, [*E. coli*]$_0$ = $10^6$ CFU $cm^{-3}$).

of coordination sites that can bind iron on the membrane or inside the cell, at relatively high iron concentrations.

Taken together, these experiments depicted the transformation trends of different iron species that occurred during bacterial inactivation. Most importantly, the results showed a significant conversion of $Fe^{3+}$ into $Fe^{2+}$ during SODIS, which might play a role in the inactivation of bacteria.

### 3.2.3. SODIS with Fe: The effect of pH

Previous experiments were conducted at near-neutral pH (6.5). To investigate the influence of the initial pH on *E. coli* inactivation with $Fe^{2+}$/$Fe^{3+}$, the pH was varied in the range of 5.0–8.0, using the optimal concentrations already identified for $Fe^{2+}$ (1 ppm, Fig. 3a) and $Fe^{3+}$ (0.25 ppm, Fig. 3b).

The results of Fig. 5 (the detailed inactivation data are shown in Fig. S2) clearly show that pH had a significant effect on bacterial inactivation in the presence of iron species under irradiation. The inactivation of *E. coli* increased gradually as the pH decreased from 8 to 5.

Indeed, pH 5 is a more hostile environment for *E. coli* survival than pH 8 is. Moreover, pH affects the distribution of dissolved iron species. Between pH 5 and 8, $Fe^{2+}$ is not the only Fe(II) species but other forms, such as $Fe(OH)^{+}$, $Fe(OH)_2^0$, and $Fe(OH)_3^-$ also occur to different extents. Furthermore, different Fe(II) species have different oxidation rate constants [13]. At pH $< 4$, $Fe^{2+}$ is the dominant form and the Fe(II) oxidation rate is unrelated to the pH. At pH $\sim 5$, the rate of oxidation depends largely on $Fe(OH)_2^0$, which is more easily oxidized than $Fe^{2+}$ or $Fe(OH)^{+}$. In the pH range 5–8, the concentration of $Fe(OH)_2^0$ increased sharply with increasing pH and the rate of Fe(II) oxidation increased accordingly. At pH values above 8, $Fe(OH)_2^0$ dominates and the oxidation rate no longer varies with the pH [56]. To quantify these differences, it has been reported that the first-order oxidation rate constants of dissolved Fe(II) species by $O_2$ differ by five orders of magnitude, as follows: $Fe^{2+}$ ($6 \times 10^{-5}$ $min^{-1}$) $< Fe(OH)^{+}$ (1.7 $min^{-1}$) $< Fe(OH)_2^0$ ($4.3 \times 10^5$ $min^{-1}$) [57]. The results shown in Fig. 5a suggest that fast Fe(II) oxidation by $O_2$ may be detrimental to disinfection [58]. In the case of $Fe^{3+}$ (Fig. 5b), increasing the pH favored the precipitation of ferric hydroxide compounds, which slowed down the inactivation of bacteria. Therefore, although Fe participates in bacterial inactivation reactions throughout the pH range of 5–8, it does so in different forms and with different reaction kinetics.

## 3.3. The combined influence of Fe and NOM on SODIS

NOM and iron species are seldom encountered separately in real water bodies. Therefore, it is important to assess their combined effects on bacterial inactivation. At pH 5, total disinfection was not achieved within 3 h of the addition of either Fe species or NOM alone (Figs. 1 and 3, respectively). In contrast, by combining $Fe^{2+}$ and NOM (Fig. 6a), the time necessary to achieve total disinfection at a pH of 5 was 120 min (SRNOM) or 150 min (NDNOM). In the case of $Fe^{3+}$, total disinfection was achieved within 180 min using either SRNOM or NDNOM. The addition of NOM to Fe improved the bacterial inactivation, suggesting that NOM enhanced the disinfection ability of the Fe species.

As noted previously $Fe^{2+}$ participates in bacterial inactivation, during which it is oxidized to $Fe^{3+}$. The latter species is less active than $Fe^{2+}$ in the inactivation process; however, when both NOM and $Fe^{2+}$ initially occur in SODIS, the resulting NOM-$Fe^{3+}$ complexes undergo rapid photoreduction to produce $Fe^{2+}$ via LMCT [13]. Similarly, after $Fe^{3+}$ addition, its coupling with NOM can enhance the rate of inactivation compared to $Fe^{3+}$ or NOM taken separately, possibly because of the photoinduced processes triggered by $Fe^{3+}$-NOM complexes. Moreover, the same complexes prevent the precipitation of $Fe^{3+}$ [22,23].

At pH 6 and 7 (Fig. 6b and c), the combination of $Fe^{2+}$ and NOM (either SRNOM or NDNOM) achieved total disinfection after 150 min (pH 6) and 180 min (pH 7). In the case of $Fe^{3+}$ and NOM, total disinfection was not achieved within 180 min, but a 5-log reduction in the bacterial population was observed after 180 min at both pH values with both NOM types.

At pH 8 (Fig. 6d), the combination of Fe and NOM was more effective for disinfection than Fe or NOM alone. However, the extent of bacterial inactivation was only slight, indicating that bacterial survival was more likely at pH 8 than at lower pH values. Part of the reason for this result might be the limited solubility of Fe at pH 8. Moreover, when the pH was below 5, the survival rate of *E. coli* was significantly limited (Fig. S3); therefore, we did not conduct further studies under lower pH conditions.

To better clarify the synergistic effect between iron species and NOM, we investigated bacterial inactivation kinetics upon irradiation in pure water, as well as in the presence of iron species alone, NOM alone, and iron + NOM at pH= 5, 6, 7, and 8. The first three bars in Fig. 7 show the action of solar light, the combined action of light + iron, and light + NOM, respectively. The stacked bars show the sum of the individual actions of the single substances (with [Fe] = [Fe + light] - [light], and a similar issue for NOM), whereas each last single-colored bar represents the combined action of light + iron + NOM.

The disinfection capacity of $Fe^{2+}$ in combination with 2 ppm SRNOM or 5 ppm NDNOM under irradiation was higher than the sum of the disinfection capacities of each factor alone, with the partial exception of pH. This result indicated that a synergistic effect occurred. Conversely, in the case of $Fe^{3+}$, the disinfection capacity of the light + $Fe^{3+}$ + NOM combination was similar to the sum of the disinfection capacities of each factor alone; thus, a synergistic effect was not discernible (except for pH 7). The catalytic cycle of $Fe^{2+}$ (oxidation to $Fe^{3+}$, followed by $Fe^{3+}$-NOM photoreduction) is probably related to the increase in *E. coli* inactivation during SODIS as well as the synergistic effect with NOM.

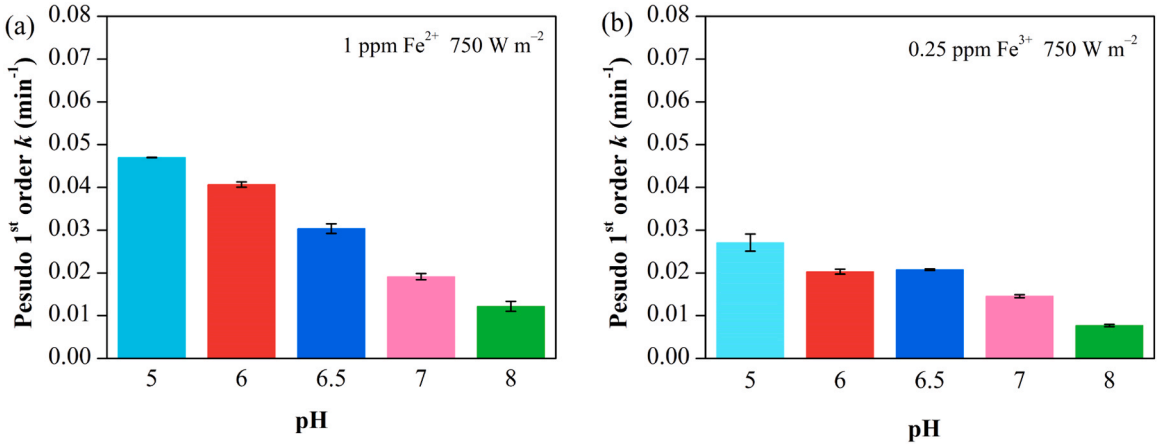


**Fig. 5.** Effects of initial pH on *E. coli* inactivation with (a) 1 ppm $Fe^{2+}$ and (b) 0.25 ppm $Fe^{3+}$ (light intensity = 750 W $m^{-2}$, $[E.\ coli]_0 = 10^6$ CFU $cm^{-3}$, pH=5–8).

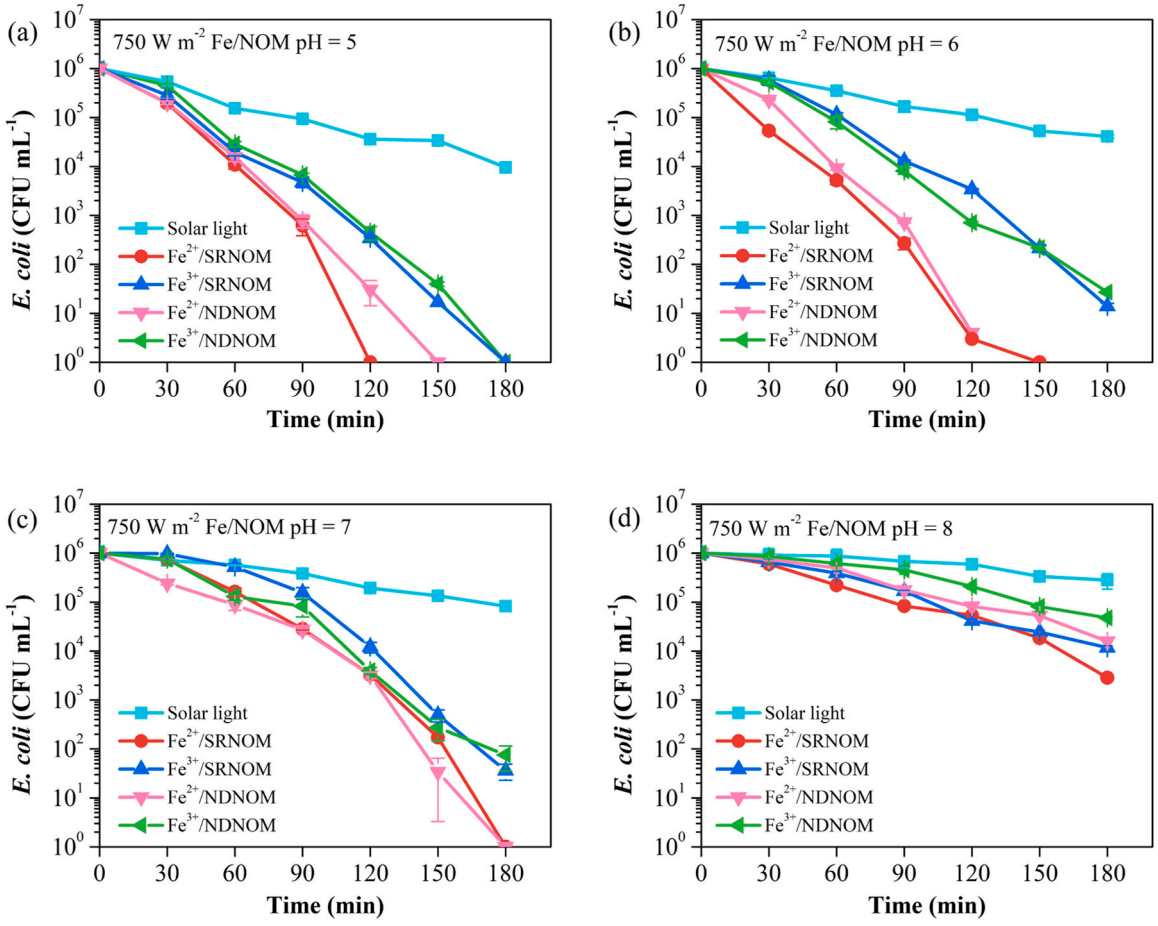


**Fig. 6.** Effects of pH on bacterial inactivation with solar light, using different combinations of NOM types and initially added iron species (a) pH= 5, (b) pH= 6, (c) pH= 7 and (d) pH= 8 (light intensity = 750 W $m^{-2}$, $[E.\ coli]_0 = 10^6$ CFU $cm^{-3}$ $[Fe^{2+}] = 1$ ppm, $[Fe^{3+}] = 0.25$ ppm, [SRNOM] = 2 ppm, [NDNOM] = 5 ppm).

### *3.4. Characterization of specific UV–vis parameters of Fe and NOM*

Fig. S4 shows the time evolution of the UV–visible absorbance spectra of the three reaction systems under irradiation: NOM alone (where NOM = SRNOM, NDNOM, SRHA, or SRFA), NOM/$Fe^{2+}$, and NOM/$Fe^{3+}$. The initial absorbance followed the order of NOM < NOM/$Fe^{2+}$ < NOM/$Fe^{3+}$. $Fe^{3+}$ considerably increases the absorbance of NOM, which is consistent with the fact that $Fe^{3+}$-NOM complexes are important chromophores [59].

Regarding the time trend of absorbance under irradiation, few changes were detected in the case of NOM alone. In contrast, an increase in the absorbance over time was apparent for NOM/$Fe^{3+}$ and NOM/$Fe^{2+}$ (Fig. S4). In the latter case, the oxidation of $Fe^{2+}$ to $Fe^{3+}$ and the subsequent complexation between $Fe^{3+}$ and NOM is likely to account for the gradual increase in chromophoric groups over the irradiation time. However, considering that different degrees of absorbance increase were observed for different types of NOM (SRNOM, NDNOM, SRHA, SRFA, and SRHA/SRFA mixtures, Fig. S5), the values and time evolution of a range of spectral parameters were investigated. The spectral parameters investigated were $E_2/E_3$, $E_2/E_4$ ($E_{270}/E_{400}$), $E_4/E_6$ ($E_{465}/E_{665}$), $SUVA_{254}$, $\varepsilon_{280}$, and $S_R$.

$E_2/E_3$ is defined as the ratio of absorbance at 254 nm to that at 365 nm. It is usually inversely proportional to NOM molecular weight and is also affected by the number of electron-donating groups [60]. $E_2/E_4$ is the ratio between the absorbance at 270 and 400 nm and provides insight into the degree of reduction of the phenolic groups in NOM [61]. Higher $E_2/E_4$ values typically indicate a higher occurrence of phenols. $E_4/E_6$ is the ratio of the absorbance at 465 and 665 nm, and it usually represents the condensation degree of the aromatic carbon network of NOM [62]. Increasing values of $E_4/E_6$ represent depletion of the aromatic NOM component. It has also been suggested that $E_4/E_6$ may be negatively correlated with NOM molecular weight; however, a review of the literature revealed no significant correlation between these parameters [63]. $SUVA_{254}$ refers to the ratio of the absorbance at 254 nm to the NOM concentration and $\varepsilon_{280}$ is the absorptivity at 280 nm. $SUVA_{254}$ and $\varepsilon_{280}$ are often used as measures of NOM aromaticity, and higher values of these parameters suggest that NOM contains more aromatic components [64]. Finally, the slope ratio, $S_R$, is linked to the fit of the spectral data (absorbance vs. wavelength) with an exponential function, considering the term at the exponent. In particular, $S_R$ is the ratio of the slope in the 275–295 nm range to the slope in the 350–400 nm range. The $S_R$ value is inversely proportional to the molecular weight of NOM [65].

The time evolution of the spectral parameters for different reaction systems is shown in Fig. 8 (data in detail: Tables S1–S10). Parameter $E_2/E_3$ (Fig. 8a and d) behaved very similarly for both SRNOM and NDNOM. In particular, the slight increase in $E_2/E_3$ in the presence of NOM alone may be due to a decrease in NOM molecular weight (fragmentation) or the consumption of electron donor groups during the irradiation process. Conversely, in the presence of $Fe^{2+}$, the $E_2/E_3$ ratio decreased with irradiation. This result might be due to the formation of chromophoric groups absorbing at relatively long wavelengths upon the oxidation of $Fe^{2+}$ to $Fe^{3+}$ (formation of $Fe^{3+}$–NOM complexes). Coherently with this hypothesis, the initial values of $E_2/E_3$ (i.e., before irradiation) followed the order NOM > NOM/$Fe^{2+}$ > NOM/$Fe^{3+}$, suggesting that $Fe^{3+}$ has a remarkable ability to lower $E_2/E_3$. In the case of NOM/$Fe^{3+}$, $E_2/E_3$ did not change during irradiation because of the small parallel increase in absorbance at 254 and 365 nm.

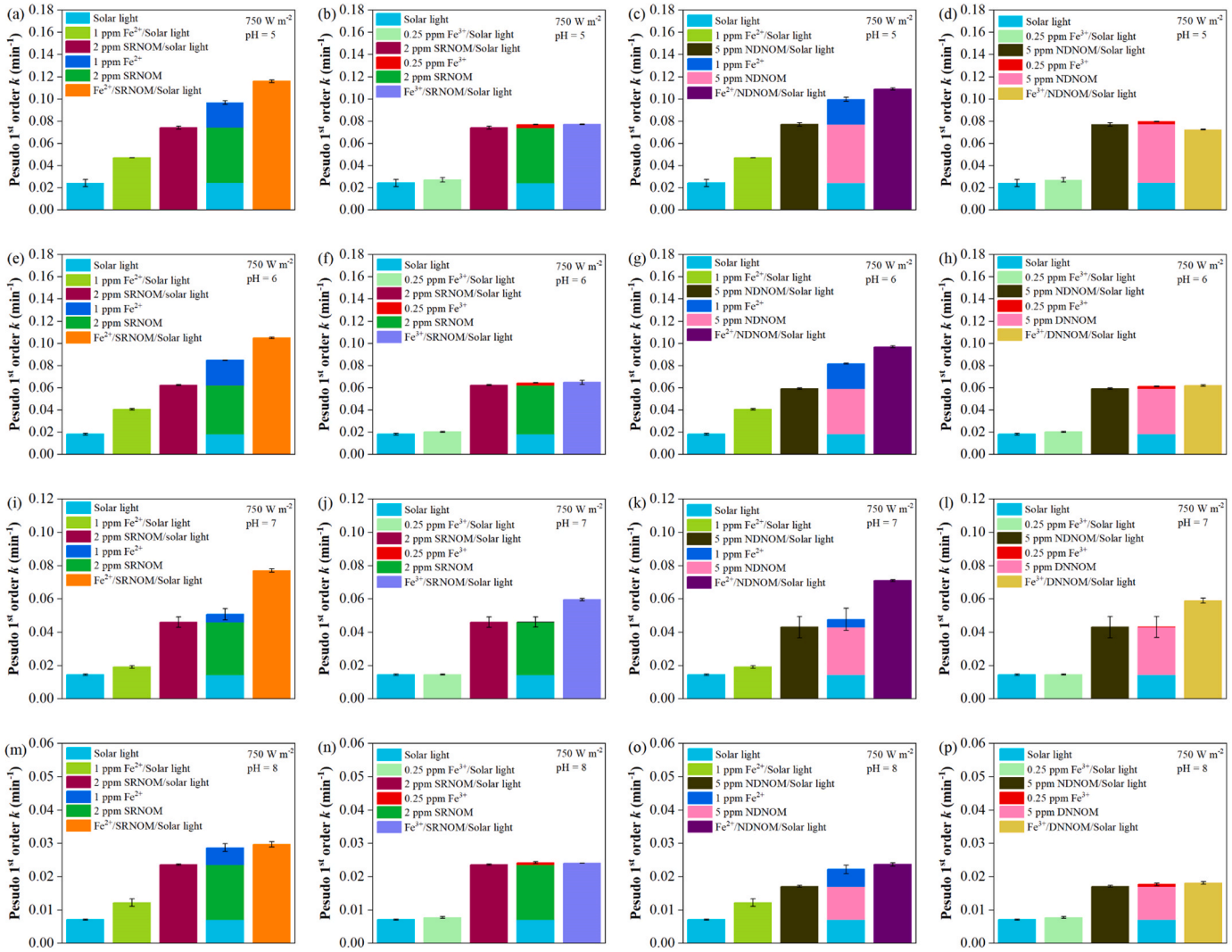


**Fig. 7.** Comparison of the pseudo-first-order rate constant of *E. coli* inactivation upon irradiation with the addition of Fe species or NOM, alone and in combination at (a-d) pH 5, (e-h) pH 6, (i-l) pH 7, and (m-p) pH 8 (light intensity = 750 W $m^{-2}$, $[E.\ coli]_0 = 10^6$ CFU $cm^{-3}$).

For $E_2/E_4$ (Fig. 8b and e), the higher initial value in the case of SRNOM alone (7.48) compared to NDNOM alone (6.78) is consistent with the known relative content of phenolic groups in the two substances (higher for SRNOM, [25]). The overall time trend of $E_2/E_4$ was similar to that of $E_2/E_3$. In particular, the $E_2/E_3$ decrease for NOM/$Fe^{2+}$ suggests that phenols may be particularly susceptible to PPRI production.

The $E_4/E_6$ ratio is a less robust indicator than the previous two ratios because of the small value of $E_6$ at the denominator, which leads to large fluctuations in the data (Fig. 8c and f). Compared to SRNOM and NDNOM, the gradual decrease in $E_4/E_6$ values with time was more apparent for SRHA and SRFA (see Fig. S6 and Table S8). Such a decrease indicates the enhancement of aromaticity, which is more easily observed in aromatic-rich substrates (HA, FA) than in the whole NOM.

For the systems containing SRNOM and NDNOM alone, the $SUVA_{254}$ and $\varepsilon_{280}$ values were essentially constant over time (Fig. 8g, j, h, and k). Conversely, both $SUVA_{254}$ and $\varepsilon_{280}$ values increased in the presence of $Fe^{2+}$ and $Fe^{3+}$. This trend suggests the formation of additional chromophoric groups or changes in the structure of the chromophores, which may be attributed to aromatic ring condensation or an increasing ratio of aromatic to aliphatic carbons. This could be due to the structures formed by the interaction between NOM and iron species [66].

The gradual increase in $S_R$ with increasing irradiation time for SRNOM and NDNOM alone (Fig. 8i and l) was linked to a parallel increase in $S_{275–295}$ and a decrease in $S_{350–400}$. This finding suggests a continuous decrease in molecular weight and the occurrence of photobleaching [65]. SRHA and SRFA exhibited similar trends (Fig. S7). Different trends were observed in the presence of Fe, particularly in the NOM/$Fe^{2+}$ system. However, the likely formation of different chromophores (e.g., $Fe^{3+}$-NOM complexes) makes the link between $S_R$ and molecular weight less straightforward than in the case of NOM alone.

Overall, the results show that the presence of iron species strongly affected the spectral absorption characteristics of NOM under simulated solar irradiation. Changes in the spectral parameters upon irradiation were particularly evident in the case of NOM/$Fe^{2+}$, which may be linked to the oxidation of $Fe^{2+}$ to $Fe^{3+}$. In addition to changes in NOM molecular weight and aromatic groups and the consumption of electron-donor compounds, modification of DOM chromophores due to the presence of iron is likely to occur in the investigated systems.

### 3.5. *Generation of PPRIs under solar light in the presence of Fe and NOM, and their contribution to disinfection*

To investigate the ability of Fe and NOM to produce different transient species and assess the contribution of these species to bacterial inactivation during irradiation, the steady-state concentrations of $^{\bullet}OH$, $^3NOM^*$, and $^1O_2$ (namely, $[^{\bullet}OH]_{ss}$, $[^3NOM^*]_{ss}$, and $[^1O_2]_{ss}$) were calculated according to the methods detailed in Text S4. The detailed

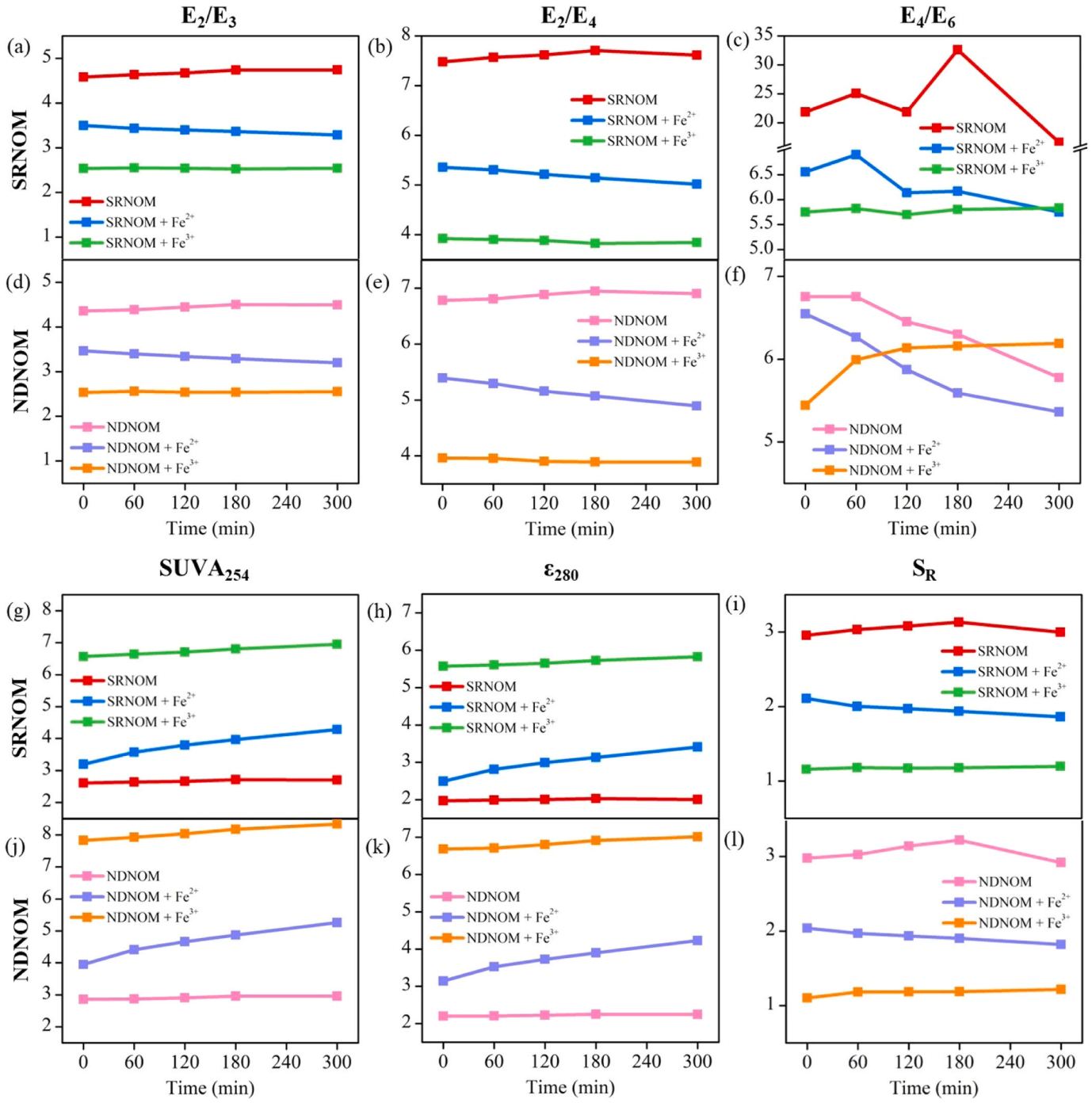


**Fig. 8.** Specific spectral parameters of (a) $E_2/E_3$ of SRNOM, (b) $E_2/E_4$ of SRNOM, (c) $E_4/E_6$ of SRNOM, (d) $E_2/E_3$ of NDNOM, (e) $E_2/E_4$ of NDNOM, (f) $E_4/E_6$ of NDNOM, (g) $SUVA_{254}$ of SRNOM, (h) $\varepsilon_{280}$ of SRNOM, (i) $S_R$ of SRNOM, (j) $SUVA_{254}$ of NDNOM, (k) $\varepsilon_{280}$ of NDNOM, and (l) $S_R$ of NDNOM over time in the absence or presence of iron species (pH=6.5, $[Fe^{2+}] = [Fe^{3+}] = [NOM] = 20$ ppm, light intensity = 750 W $m^{-2}$).

**Table 1**
The steady-state concentrations of different PPRIs in the presence of NOM and/or iron species (err. = standard error of the replicate experiments).

| | $[^{\bullet}OH]_{ss}$ M | $[^{\bullet}OH]_{ss}$ err M | $[^3NOM^*]_{ss}$ M | $[^3NOM^*]_{ss}$ err M | $[^1O_2]_{ss}$ M | $[^1O_2]^{ss}$ err M |
|---|---|---|---|---|---|---|
| 2 ppm SRNOM | 1.91E-16 | 9.22E-18 | 2.06E-14 | 1.16E-15 | 4.42E-10 | 3.47E-12 |
| 2 ppm SRNOM 1 ppm $Fe^{2+}$ | 3.45E-16 | 2.92E-17 | 2.05E-14 | 1.19E-15 | 3.27E-10 | 3.32E-12 |
| 2 ppm SRNOM 0.25 ppm $Fe^{3+}$ | 1.73E-16 | 4.48E-18 | 1.96E-14 | 2.43E-16 | 4.26E-10 | 2.21E-13 |
| 5 ppm NDNOM | 3.12E-16 | 4.42E-18 | 1.84E-14 | 1.55E-15 | 4.88E-10 | 3.47E-12 |
| 5 ppm NDNOM 1 ppm $Fe^{2+}$ | 6.24E-16 | 3.51E-18 | 2.11E-14 | 3.73E-16 | 2.87E-10 | 5.47E-12 |
| 5 ppm NDNOM 0.25 ppm $Fe^{3+}$ | 3.24E-16 | 6.99E-18 | 1.89E-14 | 1.11E-15 | 4.74E-10 | 1.99E-12 |

data are presented in Figs. S8-S11, and the results are presented in Table 1. The theoretical first-order rate constants of *E. coli* inactivation for each PPRI ($k^{1st}$) were reproduced by multiplying the $k^{2nd}$ values previously published [34] by the steady-state concentration of each relevant species [X] ($^{\bullet}OH$, $^1O_2$,$^3NOM^*$) (see Table S11). The experimental first-order rate constants for sterilization in different systems are listed in Table S12.

A comparison of the contribution of PPRI to *E. coli* inactivation suggests that $^1O_2$ likely plays a dominant role (Table S11). The theoretical values of $k^{1st}$ were higher than the experimental values, likely because of the considerable differences between PPRI reactions with organic molecules and bacteria in the presence of photosensitizers [67]. It is possible that inactivation kinetics by $^1O_2$ would not be directly proportional to [$^1O_2$] but would follow a plateau trend, which could explain the difference between the theoretical and experimental $k^{1st}$ values.

As mentioned above, UVA induces photooxidation processes, which are divided into Type I and Type II reactions. Type I reactions produce reactive species such as $^{\bullet}OH$ and $O_2^{\bullet-}$ as intermediates via electron transfer, which can lead to further $^1O_2$ formation through, e.g., oxidation of $O_2^{\bullet-}$ [68]. $Fe^{3+}$ can be regenerated into $Fe^{2+}$ through $O_2^{\bullet-}$ or $Fe^{3+}$-NOM complexes [19,69]. The Type II reaction uses NOM as a photosensitizer, transferring light energy from $^3NOM^*$ to $^3O_2$ to produce $^1O_2$ [70].

$$NOM + hv \rightarrow {}^3NOM^* + O_2 \rightarrow NOM + {}^1O_2 \quad (1)$$

$$NOM + hv \rightarrow {}^1NOM^{\bullet+/\bullet-} + O_2 \rightarrow NOM+ + O_2^{\bullet-} \quad (2)$$

$$O_2^{\bullet-} + 2H^+ \rightarrow H_2O_2 + Fe^{2+} \rightarrow Fe^{3+} + OH^- + OH^{\bullet} \quad (3)$$

$$Fe^{3+} + O_2^{\bullet-} \rightarrow Fe^{2+} + O_2 \quad (4)$$

$$Fe^{3+}\text{-}NOM + hv \rightarrow Fe^{2+} + NOM^{\bullet+} \quad (5)$$

This mechanism explains the dominant role of singlet oxygen in the inactivation process and the observed synergy between NOM and iron species, and it can also account for the unconventional [$^1O_2$] > [$^3NOM^*$], which is in agreement with other studies (see Table 1) [71–73].

The key role of $^1O_2$ as a PPRI directly involved in *E. coli* inactivation is supported by the important role played by dissolved oxygen in the process. Indeed, inactivation kinetics were considerably hampered in $N_2$ atmosphere (Fig. 9 and Table S12), while they were enhanced in systems where $H_2O$ was replaced by $D_2O$ (Table S13). In a $N_2$ atmosphere, the dominant role in inactivating bacteria is played by $^3NOM^*$, which acts as the main PPRI in such conditions.

Transient $^1O_2$ can react with amino acids (e.g., histidine and tryptophan) to affect protein function and properties. It also has similar effects (i.e., oxidative) as hydroxyl radicals and is responsible for degrading enzymes, forming protein peroxides or side-chain by-products, splitting the main chains, and inducing DNA cross-linking and aggregation [74]. The present findings suggest that singlet oxygen may play an important role in bacterial inactivation in sunlit surface waters containing iron and organic matter.

### 3.6. Synergistic role of Fe and NOM in solar irradiated waters: pathways to inactivation

Based on the experimental results and kinetic calculations, the mechanisms of the observed synergistic effect of NOM and iron on bacterial inactivation are illustrated in Fig. 10.

Solar light induces intracellular damage in *E. coli*, which can be briefly summarized as an intracellular photo-Fenton reaction and singlet oxygen production. This would result in the oxidation of the cell from the inside out. Compared to the direct irradiation effect of solar light (intracellular), the presence of NOM intensifies the transfer of solar energy and enhances extracellular/bulk bacterial inactivation by producing PPRIs such as $^3NOM^*$ and $^1O_2$. $Fe^{2+}$ can cause extensive and lethal modifications. In the absence of NOM, our findings suggest that $Fe^{2+}$ achieved a better disinfection effect than $Fe^{3+}$, although with optimum performance at slightly higher concentrations (Fig. 3).

This issue is particularly relevant for oxic waters, where dissolved Fe is mainly in the form of $Fe^{3+}$, but diurnal patterns lead to the generation of $Fe^{2+}$ under light. In SODIS, Fe addition induces the production of PPRIs, which can lead to direct oxidation of the cell membrane surface. Alternatively, the Fe species can enter the cell to induce internal Fenton reactions. However, because of the limited dissolved iron concentration usually found in natural waters and the slow cycling of $Fe^{2+}/Fe^{3+}$, the overall sterilization effect is expected to be only moderate.

The disinfection efficiency of the SODIS increased significantly when NOM was present together with Fe. When $Fe^{2+}$ produces PPRIs under irradiation, $Fe^{3+}$ is generated in the form of a NOM-$Fe^{3+}$ complex that is reduced to $Fe^{2+}$ through an LMCT process. Furthermore, the interaction between Fe(III) species and superoxide arising from NOM irradiation could be another important PPRI source. Thus, rapid light-driven $Fe^{2+}/Fe^{3+}$ cycling enhanced *E. coli* inactivation. The presence of Fe under irradiation also promoted the consumption of phenolic groups in NOM, possibly resulting in higher PPRI production rates.

## 4. Conclusions

This study demonstrated that the coexistence of Fe (especially $Fe^{2+}$) and NOM had a synergistic effect on SODIS sterilization. Based on the

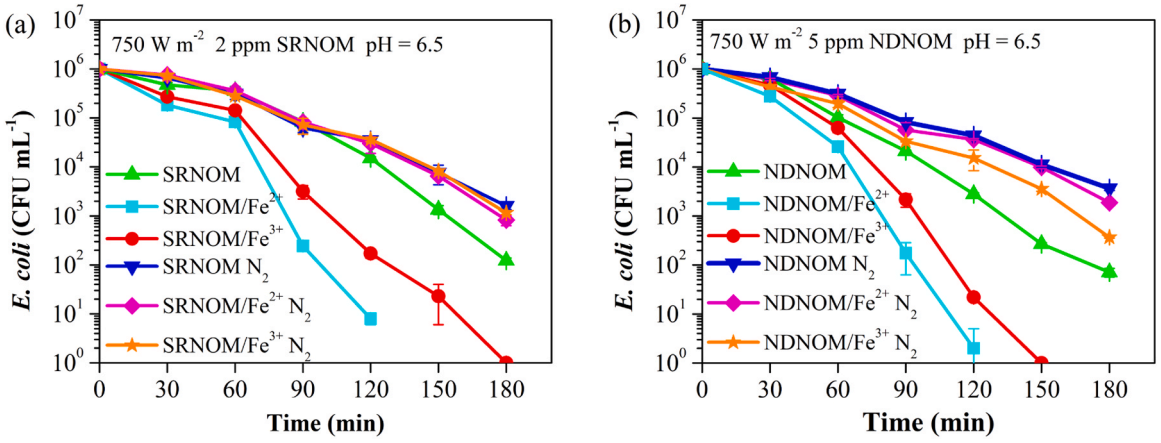


**Fig. 9.** Bacterial inactivation upon irradiation of solutions containing different types of NOM and iron species, with and without $N_2$ purging. (pH = 6.5, light intensity = 750 W $m^{-2}$, $[I]_0 = 10^6$, $[Fe^{2+}] = 1$ ppm, $[Fe^{3+}] = 0.25$ ppm, [SRNOM] = 2 ppm, [NDNOM] = 5 ppm).

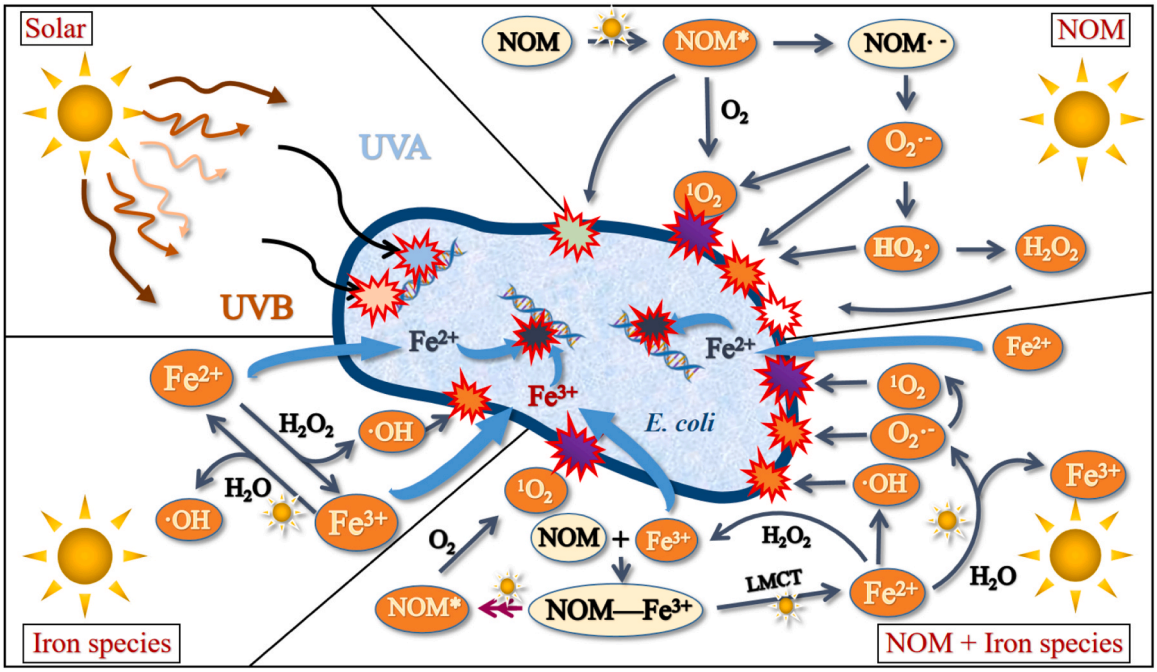


**Fig. 10.** Proposed mechanism for the enhancement of the SODIS process by the addition of NOM and iron species separately or in combination.

addition of suitable initial concentrations and types of Fe and NOM, synergistic enhancement of sterilization can be observed in the pH range of 5.0–8.0. The roles of Fe and NOM in bacterial inactivation were clarified together with their combined effects.

Presumably, a major issue is the formation of $Fe^{3+}$-NOM complexes, which retain Fe(III) in the dissolved form and exhibit photoactivity. In addition to changing the optical properties of organic matter considerably, thereby enhancing radiation absorption at long wavelengths, $Fe^{3+}$-NOM complexes are responsible for photoreduction via LMCT processes and, consequently, for $Fe^{2+}$ generation. This photoinduced pathway enhances $Fe^{2+}/Fe^{3+}$ cycling, leading to a higher production of PPRIs (among which $^1O_2$ likely has a dominating influence) and, as a result, enhances light-assisted bacterial inactivation.

The present findings suggest that in natural waters already containing Fe and NOM, the mechanisms of solar disinfection are expected to be altered compared to plain solar exposure. Under regularly encountered concentrations of NOM and Fe, both species were effective in promoting the inactivation of *E. coli* in water during solar exposure. This process forms the basic constituents of the photo-Fenton process, which can occur in the pH range of (5−8) that is typical of natural waters, indicating that NOM+Fe under light can be very germicidal even without the addition of $H_2O_2$, leading to the production of germicidal reactive species such as $^1O_2$.

## CRediT authorship contribution statement

**Da Wang**: Investigation, Data Curation, Writing - Original Draft, Visualization, Formal análisis. **Linwen Cai**: Data Curation, Writing - Original Draft, Visualization. **Shuang Song**: Resources, Writing - Review & Editing. **Stefanos Giannakis**: Supervision, Conceptualization, Writing - Review & Editing, Project administration. **Jun Ma**: Funding acquisition, Writing - Review & Editing. **Davide Vione**: Methodology, Validation, Writing - Review & Editing. **Cesar Pulgarin**: Funding acquisition, Supervision, Resources, Writing - Review & Editing.

## Declaration of Competing Interest

The authors declare that they have no known competing financial interests or personal relationships that could have appeared to influence the work reported in this paper.

## Data Availability

Data will be made available on request.

## Acknowledgements

This study was financially supported by the National Natural Science Foundation of China (Grant No. 52000158). Stefanos Giannakis acknowledges the ARPHILAKE project, "*Combating Antibiotic Resistance in Philippine Lakes: One Health upstream interventions to reduce the burden*", which received funding from the Agencia Estatal de Investigación (Spain), "Proyectos de Colaboración Internacional" (PCI2022-132918) under the umbrella of "JPIAMR - Joint Programming Initiative on Antimicrobial Resistance", as well as the REDDIS project, "*Procesos reductivos como el Talón de Aquiles bacteriano en la desinfección de aguas residuales y en aguas naturales*", which received funding from the Agencia Estatal de Investigación (Spain), "Proyectos Consolidación Investigadora 2022" (CNS2022-135728). Davide Vione acknowledges the support from Project CH4.0 under the MUR program "Dipartimenti di Eccellenza 2023–2027" (CUP: D13C22003520001).

## Appendix A. Supporting information

Supplementary data associated with this article can be found in the online version at doi:10.1016/j.apcatb.2023.123573.

## References

[1] K.G. McGuigan, R.M. Conroy, H.-J. Mosler, M. du Preez, E. Ubomba-Jaswa, P. Fernandez-Ibanez, Solar water disinfection (SODIS): a review from bench-top to roof-top, J. Hazard. Mater. 235 (2012) 29–46, https://doi.org/10.1016/j.jhazmat.2012.07.053.

[2] T.F. Clasen, L. Haller, Water Quality Interventions to Prevent Diarrhoea: Cost and Cost-effectiveness, WHO, 2008.

[3] S. Giannakis, Analogies and differences among bacterial and viral disinfection by the photo-Fenton process at neutral pH: a mini review, Environ. Sci. Pollut. R 25 (2018) 27676–27692, https://doi.org/10.1007/s11356-017-0926-x.

[4] G. McKay, K.D. Couch, S.P. Mezyk, F.L. Rosario-Ortiz, Investigation of the coupled effects of molecular weight and charge-transfer interactions on the optical and

photochemical properties of dissolved organic matter, Environ. Sci. Technol. 50 (2016) 8093–8102, https://doi.org/10.1021/acs.est.6b02109.
[5] K. Kadir, K.L. Nelson, Sunlight mediated inactivation mechanisms of Enterococcus faecalis and *Escherichia coli* in clear water versus waste stabilization pond water, Water Res. 50 (2014) 307–317, https://doi.org/10.1016/j.watres.2013.10.046.
[6] L. Lian, C. Miao, Z. Hao, Q. Liu, Y. Liu, W. Song, S. Yan, Reevaluation of the contributions of reactive intermediates to the photochemical transformation of 17 beta-estradiol in sewage effluent, Water Res. 189 (2021), 116633, https://doi.org/10.1016/j.watres.2020.116633.
[7] L. Clarizia, D. Russo, I. Di Somma, R. Marotta, R. Andreozzi, Homogeneous photo-Fenton processes at near neutral pH: a review, Appl. Catal. B Environ. 209 (2017) 358–371, https://doi.org/10.1016/j.apcatb.2017.03.011.
[8] J. Bandara, C. Morrison, J. Kiwi, C. Pulgarin, P. Peringer, Degradation/decoloration of concentrated solutions of Orange II. Kinetics and quantum yield for sunlight induced reactions via Fenton type reagents, J. Photochem. Photobio. A: Chem. 99 (1996) 57–66, https://doi.org/10.1016/1010-6030(96)04339-0.
[9] B.C. Faust, R.G. Zepp, Photochemistry of aqueous iron (III)-polycarboxylate complexes: roles in the chemistry of atmospheric and surface waters, Environ. Sci. Technol. 27 (1993) 2517–2522, https://doi.org/10.1021/es00048a032.
[10] Y. Sun, J.J. Pignatello, Photochemical reactions involved in the total mineralization of 2, 4-D by $Fe^{3+}/H_2O_2$/UV, Environ. Sci. Technol. 27 (1993) 304–310, https://doi.org/10.1021/es00039a010.
[11] A. Pulgarin, S. Giannakis, C. Pulgarin, C. Ludwig, D. Refardt, A novel proposition for a citrate-modified photo-Fenton process against bacterial contamination of microalgae cultures, Appl. Catal. B Environ. 265 (2020), 118615, https://doi.org/10.1016/j.apcatb.2020.118615.
[12] S. Giannakis, M.I.Polo Lopez, D. Spuhler, J.A. Sanchez Perez, P. Fernandez Ibanez, C. Pulgarin, Solar disinfection is an augmentable, in situ-generated photo-Fenton reaction Part 2: a review of the applications for drinking water and wastewater disinfection, Appl. Catal. B Environ. 198 (2016) 431–446, https://doi.org/10.1016/j.apcatb.2016.06.007.
[13] S. Giannakis, M.I. Polo Lopez, D. Spuhler, J.A. Sanchez Perez, P. Fernandez Ibanez, C. Pulgarin, Solar disinfection is an augmentable, in situ-generated photo-Fenton reaction-Part 1: a review of the mechanisms and the fundamental aspects of the process, Appl. Catal. B Environ. 199 (2016) 199–223, https://doi.org/10.1016/j.apcatb.2016.06.009.
[14] J. Porras, S. Giannakis, R.A. Torres-Palma, J.J. Fernandez, M. Bensimon, C. Pulgarin, Fe and Cu in humic acid extracts modify bacterial inactivation pathways during solar disinfection and photo-Fenton processes in water, Appl. Catal. B Environ. 235 (2018) 75–83, https://doi.org/10.1016/j.apcatb.2018.04.062.
[15] T.L. Theis, P.C. Singer, Complexation of iron (II) by organic matter and its effect on iron (II) oxygenation, Environ. Sci. Technol. 8 (1974) 569–573, https://doi.org/10.1021/es60091a008.
[16] B.M. Voelker, F.M. Morel, B. Sulzberger, Iron redox cycling in surface waters: effects of humic substances and light, Environ. Sci. Technol. 31 (1997) 1004–1011, https://doi.org/10.1021/es9604018.
[17] B.M. Voelker, B. Sulzberger, Effects of fulvic acid on Fe (II) oxidation by hydrogen peroxide, Environ. Sci. Technol. 30 (1996) 1106–1114, https://doi.org/10.1021/es9502132.
[18] C. Ruales-Lonfat, J.F. Barona, A. Sienkiewicz, M. Bensimon, J. Velez-Colmenares, N. Benitez, C. Pulgarin, Iron oxides semiconductors are efficients for solar water disinfection: A comparison with photo-Fenton processes at neutral pH, Appl. Catal. B Environ. 166 (2015) 497–508, https://doi.org/10.1016/j.apcatb.2014.12.007.
[19] D. Spuhler, J.A. Rengifo-Herrera, C. Pulgarin, The effect of $Fe^{2+}$, $Fe^{3+}$, $H_2O_2$ and the photo-Fenton reagent at near neutral pH on the solar disinfection (SODIS) at low temperatures of water containing *Escherichia coli* K12, Appl. Catal. B Environ. 96 (2010) 126–141, https://doi.org/10.1016/j.apcatb.2010.02.010.
[20] J. Brooks, Developing and investigating skin and wound cleaning approaches within rural Africa, J. Dermatol. Nurses Assoc. 4 (2012) 255–258, https://doi.org/10.1097/JDN.0b013e3182617a78.
[21] A. Babuponnusami, K. Muthukumar, A review on Fenton and improvements to the Fenton process for wastewater treatment, J. Environ. Chem. Eng. 2 (2014) 557–572, https://doi.org/10.1016/j.jece.2013.10.011.
[22] F. Jirsa, E. Neubauer, R. Kittinger, T. Hofmann, R. Krachler, F. von der Kammer, B. K. Keppler, Natural organic matter and iron export from the Tanner Moor, Austria, Limnologica 43 (2013) 239–244, https://doi.org/10.1016/j.limno.2012.09.006.
[23] R. Krachler, R.F. Krachler, G. Wallner, S. Hann, M. Laux, M.F.C. Recalde, F. Jirsa, E. Neubauer, F. von der Kammer, T. Hofmann, River-derived humic substances as iron chelators in seawater, Mar. Chem. 174 (2015) 85–93, https://doi.org/10.1016/j.marchem.2015.05.009.
[24] S. Papoutsakis, C. Pulgarin, I. Oller, R. Sánchez-Moreno, S. Malato, Enhancement of the Fenton and photo-Fenton processes by components found in wastewater from the industrial processing of natural products: the possibilities of cork boiling wastewater reuse, Chem. Eng. J. 304 (2016) 890–896, https://doi.org/10.1016/j.cej.2016.07.021.
[25] M. Kohantorabi, S. Giannakis, M.R. Gholami, L. Feng, C. Pulgarin, A systematic investigation on the bactericidal transient species generated by photo-sensitization of natural organic matter (NOM) during solar and photo-Fenton disinfection of surface waters, Appl. Catal. B Environ. 244 (2019) 983–995, https://doi.org/10.1016/j.apcatb.2018.12.012.
[26] J. Ma, W. Lv, P. Chen, Y. Lu, F. Wang, F. Li, K. Yao, G. Liu, Photodegradation of gemfibrozil in aqueous solution under UV irradiation: kinetics, mechanism, toxicity, and degradation pathways, Environ. Sci. Pollut. R. 23 (2016) 14294–14306, https://doi.org/10.1007/s11356-016-6451-5.
[27] D. Vione, G. Falletti, V. Maurino, C. Minero, E. Pelizzetti, M. Malandrino, R. Ajassa, R.-I. Olariu, C. Arsene, Sources and sinks of hydroxyl radicals upon irradiation of natural water samples, Environ. Sci. Technol. 40 (2006) 3775–3781, https://doi.org/10.1021/es052206b.
[28] F.L. Rosario-Ortiz, S. Canonica, Probe compounds to assess the photochemical activity of dissolved organic matter, Environ. Sci. Technol. 50 (2016) 12532–12547, https://doi.org/10.1021/acs.est.6b02776.
[29] P.H. Buehlmann, Balancing bromate formation, organics oxidation, and pathogen inactivation: The impact of bromate suppression techniques on ozonation system performance in reuse waters, Ph.D. Thesis, VA. Tech. Blacksbg., VA USA (2019).
[30] R. Scherz-Shouval, Z. Elazar, ROS, mitochondria and the regulation of autophagy, Trends Cell Biol. 17 (2007) 422–427, https://doi.org/10.1016/j.tcb.2007.07.009.
[31] E. Ortega-Gómez, M.B. Martín, B.E. García, J.S. Pérez, P.F. Ibáñez, Solar photo-Fenton for water disinfection: an investigation of the competitive role of model organic matter for oxidative species, Appl. Catal. B Environ. 148 (2014) 484–489, https://doi.org/10.1016/j.apcatb.2013.09.051.
[32] A. Garcia-Gil, L. Feng, J. Moreno-SanSegundo, S. Giannakis, C. Pulgarin, J. Marugan, Mechanistic modelling of solar disinfection (SODIS) kinetics of *Escherichia coli*, enhanced with $H_2O_2$ - part 1: the dark side of peroxide, Chem. Eng. J. 439 (2022), 135709, https://doi.org/10.1016/j.cej.2022.135709.
[33] A. Garcia-Gil, L. Feng, J. Moreno-SanSegundo, S. Giannakis, C. Pulgarin, J. Marugan, Mechanistic modelling of solar disinfection (SODIS) kinetics of *Escherichia coli*, enhanced with $H_2O_2$ - part 2: Shine on you, crazy peroxide, Chem. Eng. J. 439 (2022), 135783, https://doi.org/10.1016/j.cej.2022.135783.
[34] E.A. Serna-Galvis, J.A. Troyon, S. Giannakis, R.A. Torres-Palma, C. Minero, D. Vione, C. Pulgarin, Photoinduced disinfection in sunlit natural waters: Measurement of the second order inactivation rate constants between *E-coli* and photogenerated transient species, Water Res 147 (2018) 242–253, https://doi.org/10.1016/j.watres.2018.10.011.
[35] B.E. Cowie, V. Porley, N. Robertson, Solar disinfection (SODIS) provides a much underexploited opportunity for researchers in photocatalytic water treatment (PWT), ACS Catal. 10 (2020) 11779–11782, https://doi.org/10.1021/acscatal.0c03325.
[36] M. Castro-Alferez, M. Inmaculada Polo-Lopez, J. Marugan, P. Fernandez-Ibanez, Mechanistic modeling of UV and mild-heat synergistic effect on solar water disinfection, Chem. Eng. J. 316 (2017) 111–120, https://doi.org/10.1016/j.cej.2017.01.026.
[37] J. Cadet, T. Douki, J.-L. Ravanat, Oxidatively generated damage to cellular DNA by UVB and UVA radiation, Photochem. Photobiol. 91 (2015) 140–155, https://doi.org/10.1111/php.12368.
[38] J. Cadet, T. Douki, J.-L. Ravanat, P. Di Mascio, Sensitized formation of oxidatively generated damage to cellular DNA by UVA radiation, Photoch. Photobio. Sci. 8 (2009) 903–911, https://doi.org/10.1039/b905343n.
[39] S. Giannakis, A. Gupta, C. Pulgarin, J. Imlay, Identifying the mediators of intracellular *E. coli* inactivation under UVA light: The (photo) Fenton process and singlet oxygen, Water Res. 221 (2022), 118740, https://doi.org/10.1016/j.watres.2022.118740.
[40] D.I. Pattison, A.S. Rahmanto, M.J. Davies, Photo-oxidation of proteins, Photoch. Photobio. Sci. 11 (2012) 38–53, https://doi.org/10.1039/C1PP05164D.
[41] B. Zhang, S. Zou, R. Cai, M. Li, Z. He, Highly-efficient photocatalytic disinfection of *Escherichia coli* under visible light using carbon supported Vanadium Tetrasulfide nanocomposites, Appl. Catal. B Environ. 224 (2018) 383–393, https://doi.org/10.1016/j.apcatb.2017.10.065.
[42] M. Amin, M. Han, Roof-harvested rainwater for potable purposes: application of solar collector disinfection (SOCO-DIS), Water Res. 43 (2009) 5225–5235, https://doi.org/10.1016/j.watres.2009.08.041.
[43] J.D. Ritchie, E.M. Perdue, Proton-binding study of standard and reference fulvic acids, humic acids, and natural organic matter, Geochim. Cosmochim. Acta 67 (2003) 85–96, https://doi.org/10.1016/S0016-7037(02)01044-X.
[44] A.P.S. Batista, A.C.S. Teixeira, W.J. Cooper, B.A. Cottrell, Correlating the chemical and spectroscopic characteristics of natural organic matter with the photodegradation of sulfamerazine, Water Res. 93 (2016) 20–29, https://doi.org/10.1016/j.watres.2015.11.036.
[45] N. Walpen, M.H. Schroth, M. Sander, Quantification of phenolic antioxidant moieties in dissolved organic matter by flow-injection analysis with electrochemical detection, Environ. Sci. Technol. 50 (2016) 6423–6432, https://doi.org/10.1021/acs.est.6b01120.
[46] C.K.Y. Lau, K.D. Krewulak, H.J. Vogel, Bacterial ferrous iron transport: the Feo system, FEMS Microbiol. Rev. 40 (2016) 273–298, https://doi.org/10.1093/femsre/fuv049.
[47] N. Lopez-Vincent, A. Cruz-Alcalde, G. Moussavi, Id.C. Gonzalez, A.H. Lehmann, J. Gimenez, S. Giannakis, Improving ferrate disinfection and decontamination performance at neutral pH by activating peroxymonosulfate under solar light, Chem. Eng. J. 450 (2022), 137904, https://doi.org/10.1016/j.cej.2022.137904.
[48] C. Ruales-Lonfat, N. Benitez, A. Sienkiewicz, C. Pulgarin, Deleterious effect of homogeneous and heterogeneous near-neutral photo-Fenton system on *Escherichia coli*. Comparison with photo-catalytic action of $TiO_2$ during cell envelope disruption, Appl. Catal. B Environ. 160 (2014) 286–297, https://doi.org/10.1016/j.apcatb.2014.05.001.
[49] G. Subramanian, H. Prakash, Photo augmented copper-based fenton disinfection under visible LED light and natural sunlight irradiation, Water Res 190 (2021), 116719, https://doi.org/10.1016/j.watres.2020.116719.
[50] M. Valko, K. Jomova, C.J. Rhodes, K. Kuca, K. Musilek, Redox- and non-redox-metal-induced formation of free radicals and their role in human disease, Arch. Toxicol. 90 (2016) 1–37, https://doi.org/10.1007/s00204-015-1579-5.

[51] V. Braun, Iron uptake mechanisms and their regulation in pathogenic bacteria, Int. J. Med. Microbiol. 291 (2001) 67–79, https://doi.org/10.1078/1438-4221-00103.
[52] D. Touati, Iron and oxidative stress in bacteria, Arch. Biochem. Biophys. 373 (2000) 1–6, https://doi.org/10.1006/abbi.1999.1518.
[53] C. Pourzand, R.D. Watkin, J.E. Brown, R.M. Tyrrell, Ultraviolet A radiation induces immediate release of iron in human primary skin fibroblasts: The role of ferritin, Proc. Natl. Acad. Sci. U. S. A. 96 (1999) 6751–6756, https://doi.org/10.1073/pnas.96.12.6751.
[54] S. Kawanishi, T. Hiraku, Sequence-specific DNA damage induced by UVA radiation in the presence of endogenous and exogenous photosensitizers. Oxidants and antioxidants in cutaneous biology, in: Curr. Probl. Dermatol., 29, Karger, Basel, 2021, pp. 74–82.
[55] S. Shekoohiyan, S. Rtimi, G. Moussavi, S. Giannakis, C. Pulgarin, Enhancing solar disinfection of water in PET bottles by optimized in-situ formation of iron oxide films. From heterogeneous to homogeneous action modes with $H_2O_2$ vs. $O_2$–Part 1: iron salts as oxide precursors, Chem. Eng. J. 358 (2019) 211–224, https://doi.org/10.1016/j.cej.2018.09.219.
[56] B. Morgan, O. Lahav, The effect of pH on the kinetics of spontaneous Fe (II) oxidation by $O_2$ in aqueous solution–basic principles and a simple heuristic description, Chemosphere 68 (2007) 2080–2084, https://doi.org/10.1016/j.chemosphere.2007.02.015.
[57] F.J. Millero, The effect of ionic interactions on the oxidation of metals in natural waters, Geochim. Cosmochim. Acta 49 (1985) 547–553, https://doi.org/10.1016/0016-7037(85)90046-8.
[58] E. Kot, S. Furmanov, A. Bezkorovainy, Ferrous iron oxidation by Lactobacillus acidophilus and its metabolic products, J. Agr. Food Chem. 43 (1995) 1276–1282, https://doi.org/10.1021/jf00053a028.
[59] C. Yin, F. Meng, Y. Meng, G. Chen, Differential ultraviolet–visible absorbance spectra for characterizing metal ions binding onto extracellular polymeric substances in different mixed microbial cultures, Chemosphere 159 (2016) 267–274, https://doi.org/10.1016/j.chemosphere.2016.05.089.
[60] X. Lei, Y. Lei, J. Guan, P. Westerhoff, X. Yang, Kinetics, and transformations of diverse dissolved organic matter fractions with sulfate radicals, Environ. Sci. Technol. 56 (2022) 4457–4466, https://doi.org/10.1021/acs.est.1c08388.
[61] J. Krumins, Z. Yang, Q. Zhang, M. Yan, M. Klavins, A study of weathered coal spectroscopic properties, Energy Proc. 128 (2017) 51–58, https://doi.org/10.1016/j.egypro.2017.09.014.
[62] Y. Chen, N. Senesi, M. Schnitzer, Information provided on humic substances by $E_4/E_6$ ratios, Soil Sci. Soc. Am. J. 41 (1977) 352–358, https://doi.org/10.2136/sssaj1977.03615995004100020037x.
[63] F.J. Rodríguez, P. Schlenger, M. García-Valverde, Monitoring changes in the structure and properties of humic substances following ozonation using UV–Vis, FTIR and $^1$H NMR techniques, Sci. Total Environ. 541 (2016) 623–637, https://doi.org/10.1016/j.scitotenv.2015.09.127.
[64] J.L. Weishaar, G.R. Aiken, B.A. Bergamaschi, M.S. Fram, R. Fujii, K. Mopper, Evaluation of specific ultraviolet absorbance as an indicator of the chemical composition and reactivity of dissolved organic carbon, Environ. Sci. Technol. 37 (2003) 4702–4708, https://doi.org/10.1021/es030360x.
[65] J.R. Helms, A. Stubbins, J.D. Ritchie, E.C. Minor, D.J. Kieber, K. Mopper, Absorption spectral slopes and slope ratios as indicators of molecular weight, source, and photobleaching of chromophoric dissolved organic matter, Limnol. Oceanogr. 53 (2008) 955–969, https://doi.org/10.4319/lo.2008.53.3.0955.
[66] V. Naddeo, V. Belgiorno, R.M. Napoli, Behaviour of natural organic mater during ultrasonic irradiation, Desalination 210 (2007) 175–182, https://doi.org/10.1016/j.desal.2006.05.042.
[67] S. Mapukata, J. Britton, N. Nwahara, T. Nyokong, The photocatalytic properties of zinc phthalocyanines supported on hematite nanofibers for use against methyl orange and Staphylococcus aureus, J. Photoch. Photobio. A 424 (2022), 113637, https://doi.org/10.1016/j.jphotochem.2021.113637.
[68] Q. Yi, J. Ji, B. Shen, C. Dong, J. Liu, J. Zhang, M. Xing, Singlet oxygen triggered by superoxide radicals in a molybdenum cocatalytic Fenton reaction with enhanced redox activity in the environment, Environ. Sci. Technol. 53 (2019) 9725–9733, https://doi.org/10.1021/acs.est.9b01676.
[69] S. Giannakis, S. Liu, A. Carratalà, S. Rtimi, M. Bensimon, C. Pulgarin, Effect of Fe (II)/Fe (III) species, pH, irradiance, and bacterial presence on viral inactivation in wastewater by the photo-Fenton process: kinetic modeling and mechanistic interpretation, Appl. Catal. B Environ. 204 (2017) 156–166, https://doi.org/10.1016/j.apcatb.2016.11.034.
[70] A. Sivéry, F. Anquez, C. Pierlot, J.M. Aubry, E. Courtade, Singlet oxygen ($^1O_2$) generation upon 1270 nm laser irradiation of ground state oxygen ($^3O_2$) dissolved in organic solvents: Simultaneous and independent determination of $^1O_2$ production rate and reactivity with chemical traps, Chem. Phys. Lett. 555 (2013) 252–257, https://doi.org/10.1016/j.cplett.2012.10.063.
[71] A.C. Maizel, C.K. Remucal, Molecular composition and photochemical reactivity of size-fractionated dissolved organic matter, Environ. Sci. Technol. 51 (2017) 2113–2123, https://doi.org/10.1021/acs.est.6b05140.
[72] M. Grandbois, D.E. Latch, K. McNeill, Microheterogeneous concentrations of singlet oxygen in natural organic matter isolate solutions, Environ. Sci. Technol. 42 (2008) 9184–9190, https://doi.org/10.1021/es8017094.
[73] S.A. Timko, C. Romera-Castillo, R. Jaffé, W.J. Cooper, Photo-reactivity of natural dissolved organic matter from fresh to marine waters in the Florida Everglades, USA, Environ. Sci.: Process. Impacts 16 (2014) 866–878, https://doi.org/10.1039/C3EM00591G.
[74] M.J. Davies, Singlet oxygen-mediated damage to proteins and its consequences, Biochem. Bioph. Res. Co. 305 (2003) 761–770, https://doi.org/10.1016/S0006-291X(03)00817-9.